Atomic insights into hydrodesulfurization

Prabhu, M.K.

Chapter 3

Structural Characterization of a Novel 2D Material: Cobalt Sulfide Sheets on Au(111)

This chapter is based on:

Prabhu, M. K.; Boden, D.; Rost, M. J.; Meyer, J.; Groot, I. M. N. Structural Characterization of a Novel Two-Dimensional Material: Cobalt Sulfide Sheets on Au(111). J. Phys. Chem. Lett. 2020, 11, 21, 9038–9044

Abstract

Transition metal dichalcogenides (TMDCs) are a type of 2D materials widely investigated by both experimentalists and theoreticians, because of their unique properties. In the case of cobalt sulfide, density functional theory (DFT) calculations on freestanding S-Co-S sheets suggest there are no stable 2D cobalt sulfide polymorphs, whereas experimental observations clearly show TMDC-like structures on Au(111). In this study we resolve this disagreement by using a combination of experimental techniques and DFT calculations, considering the substrate explicitly. We find a 2D CoS_2 sheet with a CoS(0001)-like atomic structure on Au(111) that delivers excellent agreement between theory and experiment. Uniquely, this sheet exhibits a metallic character, contrary to most TMDCs, and exists due to the stabilizing interactions with the Au(111) substrate.

3.1 Introduction

Transition metal dichalcogenides (TMDCs) are a class of 2D materials that have been extensively researched over the last two decades, because of their unique chemical and mechanical properties for applications in (opto)electronics, biology, high-density storage, efficient energy harvesting, high-resolution imaging, and catalysis.[1–7] The scientific community has been on a quest to discover new TMDCs with unique properties to improve existing applications as well as to find completely new ones. Currently, the metals of groups 4 to 6 and those of group 10 are thoroughly investigated, because in the bulk, they form layered TMDCs held together by Van der Waals forces.[8] The weak Van der Waals forces enable mechanical or chemical exfoliation of 2D sheets from the bulk materials.[9]

Higher-quality single-layer TMDCs can also be synthesized by epitaxial growth on a suitable substrate, for example single-layer TMDCs of Mo,[10] W,[11] Ti,[12] Ta,[13] Zr,[14] Nb[15] and Hf.[16] Gold substrates are a preferred choice to grow many of these single-layer TMDCs as the high chalcogen affinity of gold can have a stabilizing effect.[17] Consequently, in order to properly investigate the existence and specific properties of potential TMDCs, interactions with the support must be considered.

Theoretical methods, such as density functional theory (DFT), are a powerful tool to predict new TMDC candidates with unique properties. However, the support is often not considered, which causes a major discrepancy between calculations and reality and limits the scope of the predictions. For instance, Ataca et al.[18] investigated most of the transition metals for their ability to form TMDCs using freestanding sheets in vacuum. They found that cobalt sulfide does not form stable TMDC sheets. This stands in disagreement with some experimental work by Kibsgaard et al.[19], who show TMDC-like cobalt sulfide sheets are formed on Au(111) after exposing cobalt nanoparticles to H_2S.

In this work we demonstrate that, when including the Au(111) substrate explicitly in our DFT calculations, excellent agreement between experiment and theory can be achieved for 2D cobalt sulfide. We obtain an atomic model for the cobalt sulfide sheets which nicely fits with our experimental results from scanning tunneling microscope (STM), low-energy electron diffraction (LEED) and X-ray photoelectron spectroscopy (XPS). Our structure, which is similar to bulk-terminated CoS(0001), improves the model suggested by Kibsgaard et al.[19]. In addition, the methodology used in our research could potentially be applied to other earth-abundant transition metals such as Fe, Ni, and Cu in order to explore the existence of other novel 2D materials.

3.2 Experimental details

All experiments were carried out in the *ReactorSTM*[20] in ultra-high vacuum (UHV) mode. An Au(111) single crystal was prepared by repeated cycles of sputter cleaning with Ar^+ ions (1.5 keV) and annealing to 873 K. Two-dimensional cobalt sulfide was grown by depositing cobalt in an H_2S atmosphere of 2×10^{-6} mbar onto the clean Au(111) single crystal maintained at 410 K. Thereafter, the sample was annealed to 650 K for 20 minutes and cooled down within 10 minutes to 473 K in the H_2S atmosphere. Lastly the sample was cooled down to 300 K within 120 minutes in UHV.

All STM imaging was performed with a tunneling current of ∼100 pA and a sample voltage of −1 V with the sample held at room temperature in UHV. To enhance the visibility of the details, we display

the STM images with a line-by-line background subtraction. Note, however, that the height profiles are obtained from STM images with planar background filtering on the entire image ensuring a correctly connected 2D surface. All post-processing is carried out using in-house developed software (*CAMERA* v4.3.5) as well as *WSXM*.[21] LEED experiments were performed using a commercial *Omicron SPECTALEED*. The diffraction images were obtained with a *Canon EOS50D* camera using manual focusing and a 30-second exposure time. The LEED images shown here were contrast-enhanced further in RAW format without any other processing. The XPS spectra were measured using the SPECS-Phoibos system with a *HSA 3500* hemispherical analyzer. A monochromator was used to select Al K-alpha radiation with a 1486.7 eV excitation energy and an incidence angle of 54.6 degrees was used. The spectra of S 2*p* and Co 2*p* were acquired with a pass energy of 20 eV and integrated 25 times to improve the signal-to-noise ratio. After acquisition, a Shirley background was subtracted using the *CASA XPS* software. To calculate the stoichiometry of 2D cobalt sulfide, the peak areas were corrected for their relative sensitivity factors.[22]

3.3 Computational Details

All DFT calculations were performed with the Vienna Ab Initio Simulation Package (VASP, version 5.2)[23–26] in combination with the Atomic Simulation Environment (ASE, version 3.19)[27] for generating input and analyzing output files. After having verified that spin-polarization is not relevant for CoS (bulk structure) and CoS_2 (bulk structure) consistent with earlier results,[28] the non-spin-polarized formulation of the PBE exchange correlation functional[29] has been used for all the surface calculations.

The Kohn-Sham orbitals were expanded into a plane-wave basis set with a cut-off energy of 300 eV, and ion-electron interactions were described by the projector-augmented wave method (PAW dataset 52 from 2012[30,31]). 12 × 12 × 12, 7 × 7 × 7 and 9 × 9 × 9 Monkhorst-Pack k-point grids[32] have been used for the aforementioned CoS, CoS_2 and fcc-Au bulk structures, respectively, resulting in the equilibrium lattice constants $a_{CoS}^{DFT} = 3.35$ Å (with $a_{CoS}^{DFT} / c_{CoS}^{DFT} = 2/3$), $a_{CoS2}^{DFT} = 5.49$ Å, and $a_{Au}^{DFT} = 4.16$ Å. This is in good agreement with the corresponding experimental values $a_{CoS}^{exp} = 3.38$ Å (with $a_{Au}^{exp} / c_{Au}^{exp} = 2/3$)[33], $a_{CoS2}^{exp} = 5.54$ Å[34] and $a_{Au}^{exp} = 4.07$ Å[35] which is expected for the PBE functional.[36] Despite this good agreement, differences between experimental and theoretical lengths remain, therefore in this work all distances discussed concern experimental values unless explicitly stated otherwise. Surface structures were based on a relaxed four-layer slab model for unreconstructed Au(111) with surface lattice constant $a_{Au(111)}^{DFT} = \frac{\sqrt{2}}{2} a_{Au}^{DFT}$. For the ensuing relaxations of the large-scale cobalt sulfide overlayer structures the bottom three gold layers were frozen. For all these calculations a maximum force threshold of 10^{-3} eV/ Å has been used, together with a vacuum distance of ≥ 8 Å and Monkhorst-Pack[32] k-point grids corresponding to at least 13 x 13 x 1 k-points in the primitive Au(111) unit cell. STM images have been simulated according to the Tersoff-Hamann approach[37] as implemented in the HIVE-STM software package[38] by plotting a surface of constant density of states within 0.05 eV of the reported bias voltage.

3.4 Results and discussions

Figure 1a shows the STM image of large 2D cobalt sulfide sheets grown on Au(111). The terraces of Au(111) no longer show the typical herringbone reconstruction after exposure to H_2S (see the SI). An identical distorted herringbone reconstruction of Au(111) upon exposure to H_2S has been observed in the experiments of Kibsgaard et al.[19] and also in low-coverage thiol[39–41] and hexabromobenzene[42] adsorption experiments performed by other research groups. Upon flash annealing to 673 K in UHV, the typical herringbone reconstruction is partially restored while the cobalt sulfide sheets remain intact (see SI). Furthermore, the height line A indicated in Figure 1a and shown in Figure 1b reveals that the cobalt sulfide sheet has an average thickness of 2.43 Å with corrugations of ± 0.2 Å in comparison to the experimental Au-Au step height of 2.32 Å.

The 2D cobalt sulfide grows as large pristine sheets into and out of the step edges of Au(111). The boundary-line of the 2D cobalt sulfide sheets has a curved shape along the Au-cobalt sulfide interface and the 2D cobalt sulfide step edge. Analysis of the contact angles between the line interfaces at the two triple points of the cobalt sulfide sheets reveals a mirror symmetry (see SI). The corresponding triple points of different cobalt sulfide sheets however, have surprisingly the same contact angles irrespective of the size of the sheets. This shows that the interfacial tension at the triple points of the interfaces are responsible for the observed shape of the cobalt sulfide islands. We think that the mirror symmetry arises from different edge terminations at the two triple points, however, further investigations into the interactions at the Au and 2D cobalt sulfide line interface are beyond the scope of this work.

The cobalt sulfide sheets have a hexagonal structure in their basal plane which has been further resolved in Figure 1c. This hexagonal structure consists of a rhombus-shaped unit cell marked in blue with six bright spots along its edges. This unit cell has a side length of 1.97 nm, which corresponds to 7 Au-Au inter-atomic distances. We therefore classify this structure as a (7x7) cobalt sulfide structure with respect to Au(111). This (7x7) structure is further demonstrated by the LEED pattern of the cobalt sulfide sheets shown in Figure 1d. The bright spots encircled in blue arise from the bare Au(111) surface. The small satellite spots expected for Au(111) are reduced to spot-broadening (see inset, 1d) due to the aforementioned modification of the herringbone reconstruction caused by the exposure to hydrogen sulfide. The smaller spots can be attributed to the Co sulfide sheets and show a hexagonal (7x7) symmetry with respect to the Au(111) spots in agreement with the STM results. The rhombus-shaped unit cell consists of two triangular halves, as indicated by a green dotted line in the inset of Figure 1c. One of the triangular halves (upper right one) has a higher relative contrast than the other (lower left one), causing the contrast to alternate in a hexagonal pattern. Additionally, the vertices of the rhombus-shaped unit cell appear dark in the STM image. Atomic resolution in Figure 1c reveals that the distances between the bright spots in the top layer of the cobalt sulfide of ~3.3 Å are similar to what was found by Kibsgaard et al.[19], who attributed this pattern to a sheet-like structure similar to $Co_3S_4(111)$.

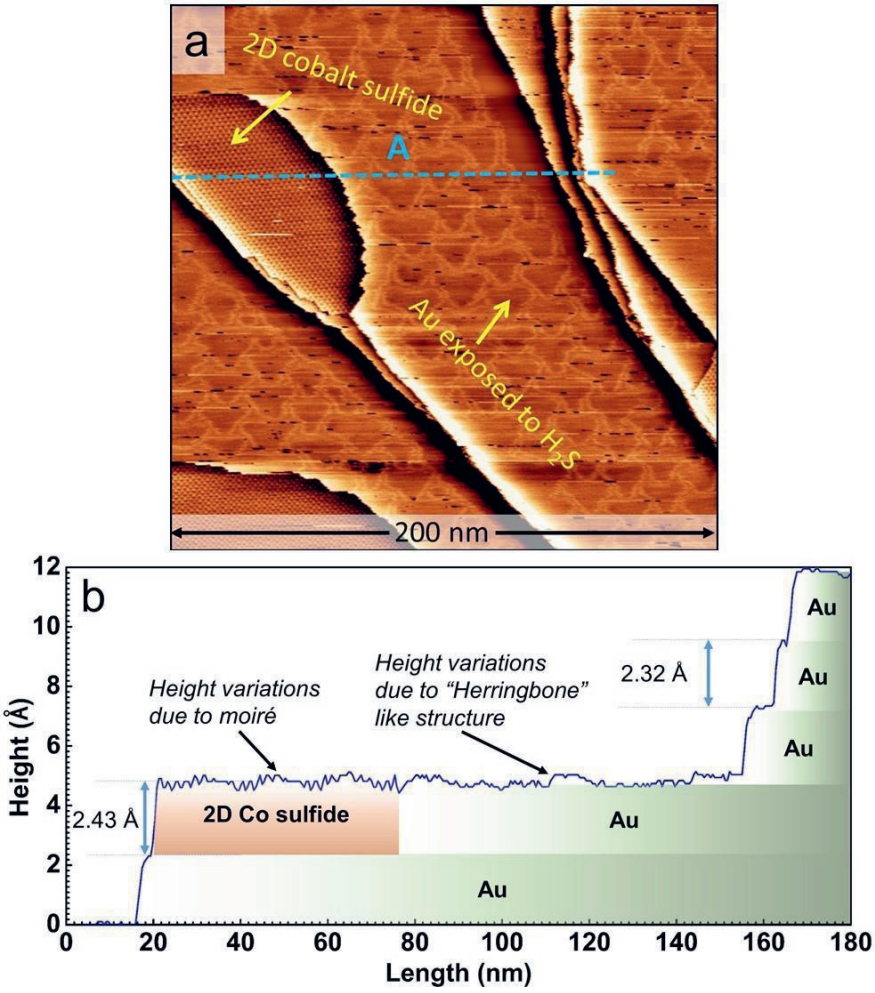
a
2D cobalt sulfide
A
Au exposed to H_2S
200 nm
b
Height variations due to moiré
Height variations due to "Herringbone" like structure
2.32 Å
2.43 Å
2D Co sulfide
Au
Au
Au
Au
Height (Å)
Length (nm)
0
2
4
6
8
10
12
0
20
40
60
80
100
120
140
160
180

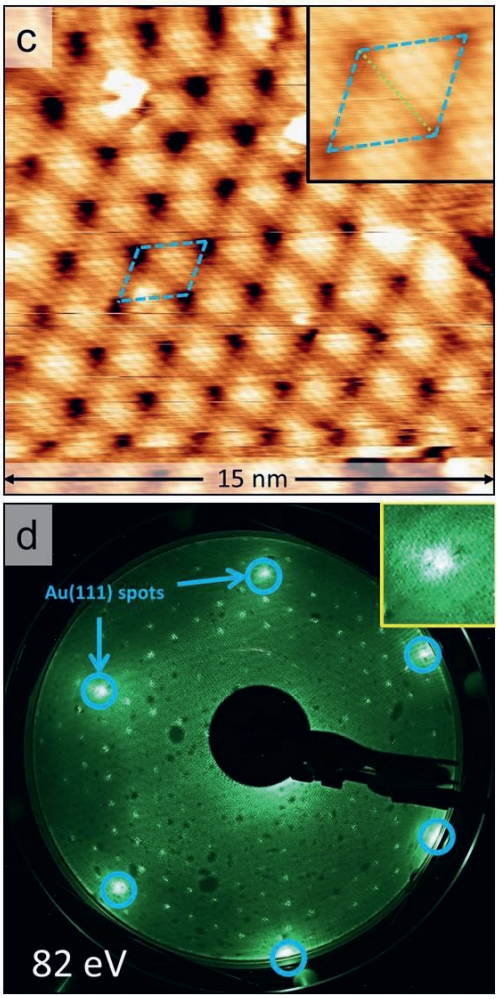

Figure 1: 2D cobalt sulfide supported on Au(111); (a) Large-scale STM image showing single-layer cobalt sulfide sheets. A modified reconstruction of Au(111) due to H_2S exposure with a long-range hexagonal arrangement is seen on the steps of gold. The respective phases are marked in the Figure. (b) Measured height profile along the blue dashed line marked A in (a). (c) Atomically-resolved STM image of the 2D cobalt sulfide. The rhombus-shaped unit cell is shown in blue with the two triangular halves demarcated by a green dotted line and enlarged in the inset for increased clarity. Image acquired at sample voltage of -0.7 V. (d) LEED pattern of cobalt sulfide sheets on Au(111) with an incident energy of 82 eV. The diffraction spots of the Au(111) surface are indicated by blue circles. Inset shows a zoom-in of the Au spot which shows that the spots due to herringbone reconstruction are reduced to spot broadening.

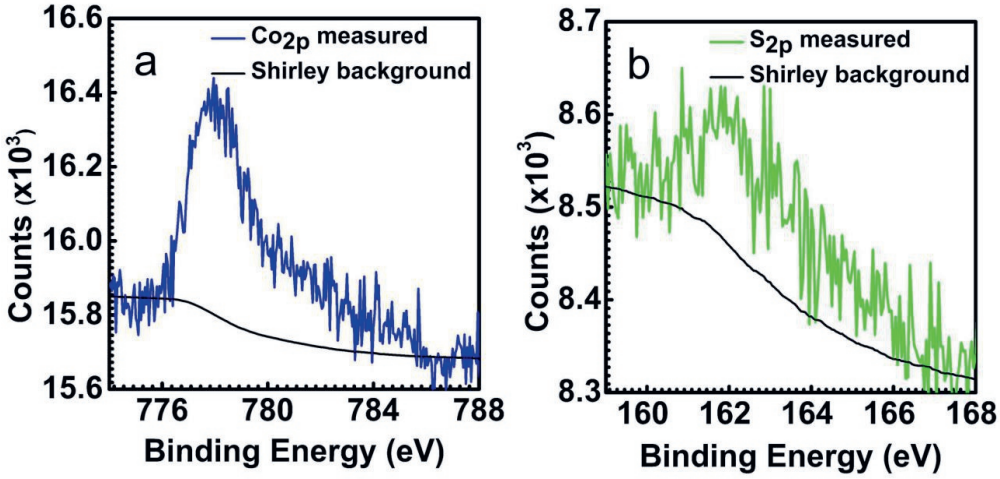

Figure 2: XPS spectra of 2D cobalt sulfide supported on Au(111) after flash annealing to 673 K to remove sulfur species adsorbed on the Au(111) terraces. (a) Co $2p_{3/2}$. (b) S $2p$.

To determine the stoichiometry of the cobalt sulfide sheets, the sample was flash annealed to 673 K in UHV in order to desorb the sulfur species on the Au(111) terraces. After this step, XPS spectra were measured (shown in Figure 2). The relative areas of the Co $2p_{3/2}$ and S $2p$ peaks were corrected by the surface relative sensitivity factors[22] to determine the Co : S ratio. Our measurements show a ratio of Co : S = 1 : 2.09 suggesting that the sheets are of the form CoS_2(see SI for details), while an approximate ratio of Co : S = 1 : 2.7 has been reported by Kibsgaard et al. using Auger electron spectroscopy.[19]

We used the experimental findings in this work and that of Kibsgaard et al. along with DFT calculations to arrive at an atomic model. A logical first structure is a sheet based on $Co_3S_4(111)$, as this is one of the most common bulk-terminated, hexagonal, cobalt sulfide surfaces reported in literature.[43] The experimental unit cell of $Co_3S_4(111)$ is 6.65 Å$\times$ 6.65 Å and the lateral S-S distance is 3.3 Å, which matches with the distance of 3.3 Å between the bright spots in the STM image in Figure 1c.[43] As discussed previously, the unit cell from LEED and STM corresponds to 7 $\times$ 7 gold atoms, which is only ~1.3% smaller than the experimental size of 3 $\times$ 3 $Co_3S_4(111)$ unit cells. To create a model for the cobalt sulfide sheet on gold, the top S-Co-S layers of a 3 $\times$ 3 $Co_3S_4(111)$ supercell are fitted onto a 7 $\times$ 7 Au(111) surface. As shown in Figure 3a, this results in an S-Co-S "sandwich" structure with a Co : S = 3 : 8 stoichiometry that is very similar to what was suggested by Kibsgaard et al.[19]. However, this $Co_3S_4(111)$-like structure proved unstable during relaxation with DFT. The simulated STM image of the resulting "rearranged" $Co_3S_4(111)$-like sheet shown in Figure 3b and the experimental STM image in Figure 1c showed no similarities. For details of the DFT relaxation, see the SI.

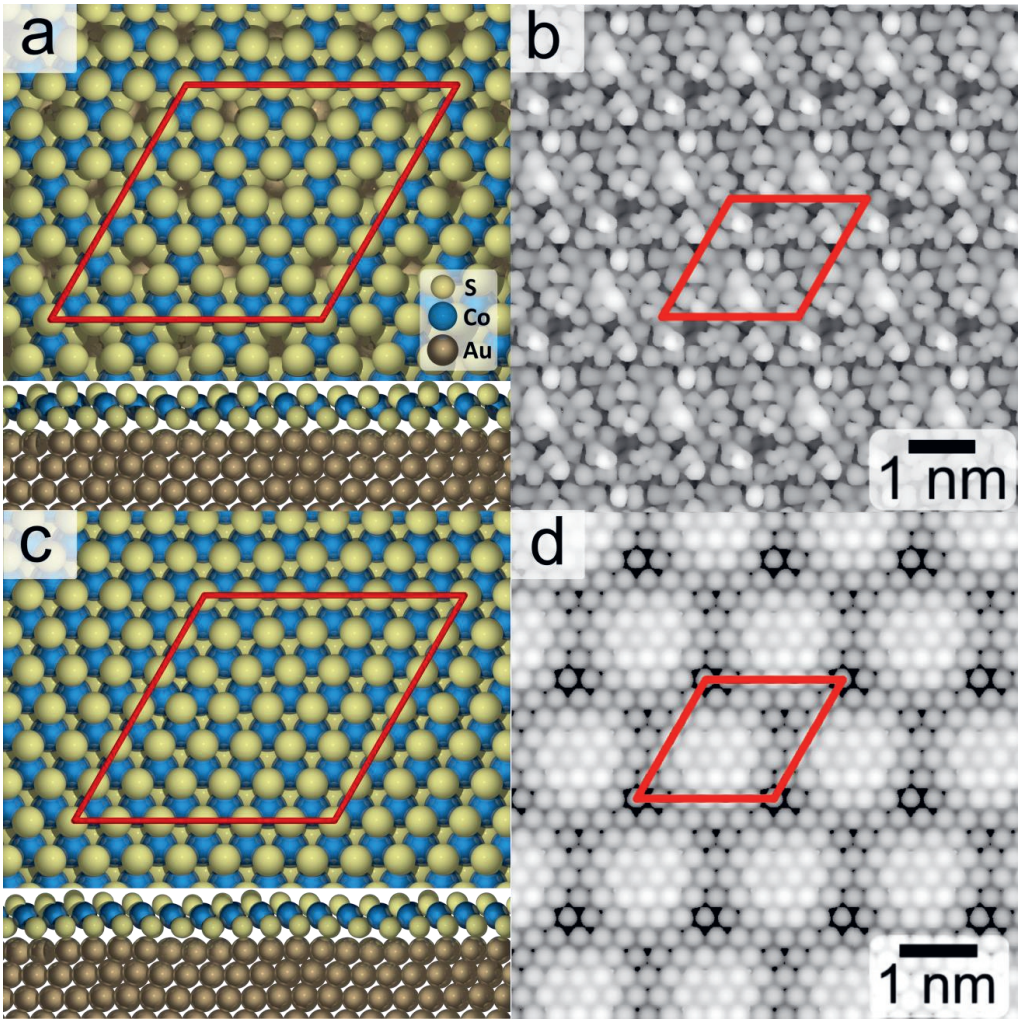

Figure 3: Schematic models of 7×7 overlayer structures on Au(111) comprised of (a) Co_3S_4(111)-like and (c) CoS(0001)-like S-Co-S sheets, each with a top (side) view in the upper (lower) part of the image. (b, d) Simulated STM images of the structures resulting from relaxation of (a) and (c), respectively. Both images were simulated using the Tersoff-Hamann method with a bias-potential of -0.3 V. The contrast has been adjusted for better comparison with Figure 1c. The unit cells in (a)-(d) are indicated in red.

CoS(0001) is another bulk-terminated cobalt sulfide surface having a hexagonal unit cell with an experimental unit cell size of 3.38 ˚A × 3.38 ˚A.[33] This means a 6 × 6 supercell of bulk-terminated CoS(0001) is ∼2.9% larger than the experimentally found unit cell of the cobalt sulfide sheet in Figure 1c. A schematic model of the CoS(0001)-like 2D CoS_2 sheet on Au(111) is shown in Figure 3c. It is very similar to the Co_3S_4(111)-like sheet, however, there are no holes in the Co layer, resulting in a Co : S = 1 : 2 stoichiometry. This matches the experimentally determined Co : S ratio of 1 : 2.09 more closely than the Co_3S_4(111)-like sheet. Furthermore, the 2D CoS_2 sheet remains stable during relaxation with DFT and the simulated STM image shown in Figure 3d reproduces most of the key features in the experimental STM image in Figure 1c. We note that the simulated STM images have a significantly higher resolution than is achievable in an STM experiment because no tunneling integral is included accounting for the finite tip size. Comparison of the bond distances in Table 1 reveals that the bond distances within the CoS(0001)-like 2D CoS_2 sheet remain similar to experimental values found in both bulk Co_3S_4 and CoS after relaxation with DFT, especially considering the known disparity stemming from the approximations in the DFT functional as discussed in the Computational Details section.

Because 6 lateral S-S distances in the 2D CoS_2 sheet are equivalent to 7 Au-Au distances along the Au(111) surface, a moiré pattern forms during relaxation with DFT featuring the striking bright and dark triangles seen in the STM images (1c), as well as the darker spots at the vertices. When the sulfur in the bottom layer sits close to the top of the underlying Au atom, it is slightly elevated (up to 0.5 Å) compared to the sulfur atom near the hollow or bridge sites, as is clearly visible in Figure 4. This causes a small corrugation in the entire cobalt sulfide sheet, which is exaggerated in the top sulfur layer. This leads to the brighter and darker areas in the STM images displayed in Figure 1c and Figure 3d.

Table 1: Average bond distances from the structure shown in Figure 3(c) after relaxation compared to corresponding bond distances in bulk cobalt sulfides and thiols on Au(111). Theoretically and experimentally obtained values are indicated with *T* and *E*, respectively

Structure	$d_{Au\text{-}S}$ (Å)	$d_{Co\text{-}S\ (bottom)}$ (Å)	$d_{Co\text{-}S(top)}$ (Å)	$d_{Co\text{-}Co}$ (Å)
CoS(0001)-like 2D CoS_2 sheet/Au(111) *T*	2.57	2.24	2.25	3.43
Bulk Co_3S_4[43,44] *E*	-	2.27	2.27	3.33
Bulk CoS[33] *E*	-	2.33	2.33	3.37
Thiols[45,46] *T*	2.63 (0.18)	-	-	-

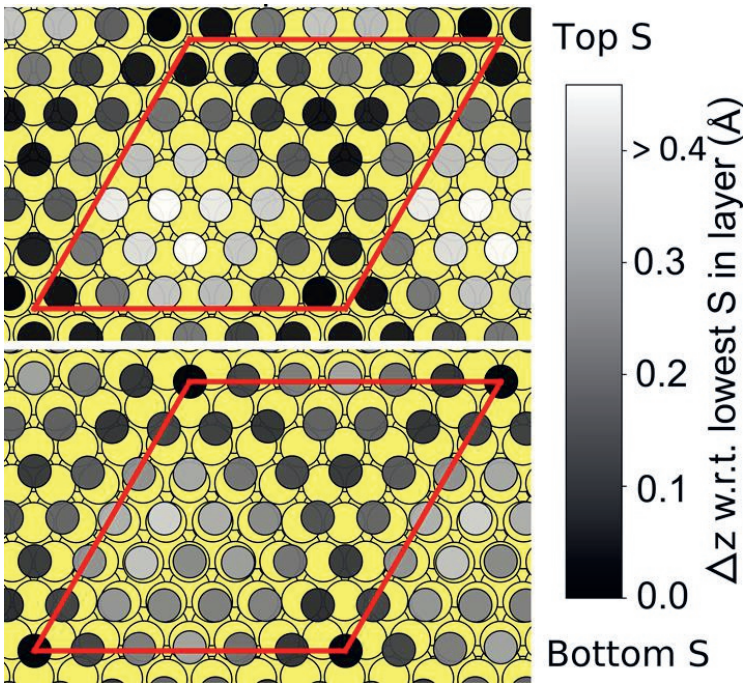

Figure 4: The positions of the sulfur atoms in the top and bottom basal planes of the cobalt sulfide sheet from Figure 3c. The gold atoms are shown in yellow, while the height of the sulfur atoms relative to the lowest atom in each respective layer is indicated in gray scale. The unit cell is displayed as a red rhombus. The height variation in the bottom layer of sulfur atoms due to the lattice mismatch with gold is exaggerated in the top layer. Comparison with Figure 3d indicates the distinct pattern can be explained by height variations of atoms in the top layer, rather than any electronic effect.

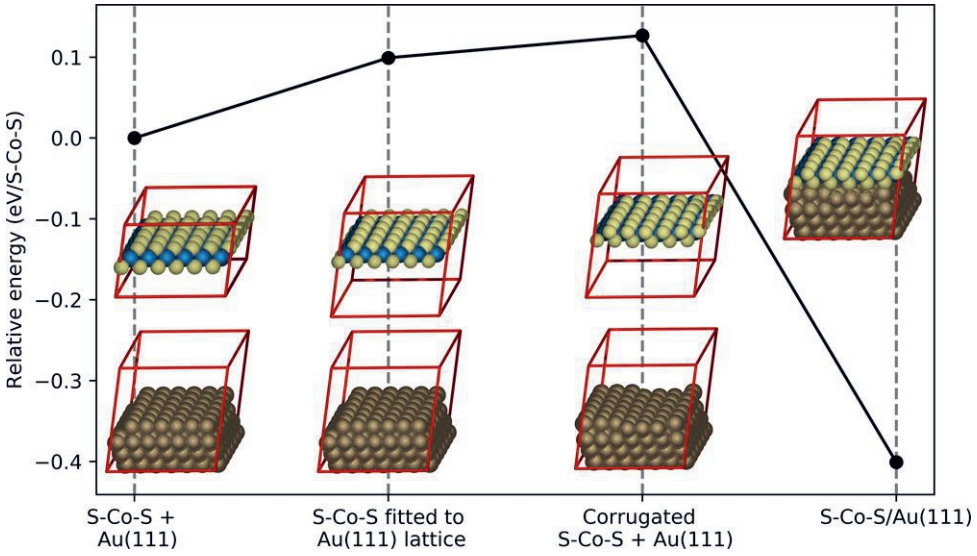

Figure 5: Decomposition of the interaction energy for the cobalt sulfide sheet and Au(111) as obtained from DFT calculations. Energies are per S-Co-S unit, with the separated Au(111) slab and freestanding S-Co-S film in equilibrium geometry shown in the leftmost inset defining the energy zero. Further from left to right: Separated Au(111) slab and freestanding S-Co-S film compressed by 1% to coincide with 7/6 Au(111) surface lattice constants, same as before but additionally including the interfacial corrugation of the structure where the S-Co-S film and Au(111) are in contact, which is finally the case in the rightmost relaxed 7x7 S-Co-S overlayer structure on Au(111) (i.e. same structure as schematically depicted in Figure 3c).

Unlike MoS_2 and TiS_2, no layered bulk structure has been reported for Co sulfide, whereby the interaction between layers consists of Van der Waals forces only, has been reported for cobalt sulfide. The cobalt sulfide bulk structure that most closely resembles MoS_2 and TiS_2 is the previously discussed CoS bulk structure. However, single-layer cobalt sulfide sheets cannot be obtained by exfoliation of a CoS crystal, because the layers are held together by covalent bonds.[17] Nevertheless, we demonstrate that 2D CoS_2 sheets with an S-Co-S structure can be synthesized on Au(111). Figure 5 shows that the interaction energy of the 2D CoS_2 sheet with the Au(111) surface is -0.40 eV per sulfur atom in the bottom layer according to our DFT calculations. This is very similar to the strong Au-S bond of thiols chemisorbed on Au(111),[45,46] as also further corroborated by the similarities in the bond lengths (see Table 1). The substantial interaction between gold and the 2D CoS_2 sheet can also be discerned from the band structure and the (projected) densities of states available in the SI, which also reveals the metallic nature of the 2D CoS_2 sheet. The formation of 2D CoS_2 sheets on the Au(111) surface may be facilitated by the strong interaction between sulfur and gold, despite the presence of Co. This interaction appears covalent in nature, since there is almost no net charge transfer between the gold and the cobalt sulfide sheet (see SI for more details).

In summary, we show that two-dimensional cobalt sulfide forms on Au(111) with a S-Co-S structure. The formation of 2D cobalt sulfide on Au(111) is facilitated by strong Au-S interactions. The nature of the electronic interaction of cobalt sulfide with the Au(111) substrate is similar to that of MoS_2, however, unlike MoS_2, cobalt sulfide does not have a band gap. Since most TMDCs are semiconductors, cobalt sulfide stands out in this regard which opens up possibilities for novel applications. In the case of 2D cobalt sulfide on Au(111), theory and experiment only agree when the substrate is considered explicitly in DFT calculations. This means that, when looking for potential new 2D materials, reliance solely on gas-phase calculations is not sufficient and a more complete approach is required.

3.5 References

(1) Jariwala, D.; Sangwan, V. K.; Lauhon, L. J.; Marks, T. J.; Hersam, M. C. Emerging Device Applications for Semiconducting Two-Dimensional Transition Metal Dichalcogenides. *ACS Nano*. 2014, pp 1102–1120. https://doi.org/10.1021/nn500064s.

(2) Chhowalla, M.; Shin, H. S.; Eda, G.; Li, L. J.; Loh, K. P.; Zhang, H. The Chemistry of Two-Dimensional Layered Transition Metal Dichalcogenide Nanosheets. *Nature Chemistry*. 2013, pp 263–275. https://doi.org/10.1038/nchem.1589.

(3) Geim, A. K.; Grigorieva, I. V. Van Der Waals Heterostructures. *Nature*. 2013, pp 419–425. https://doi.org/10.1038/nature12385.

(4) Lightcap, I. V.; Kosel, T. H.; Kamat, P. V. Anchoring Semiconductor and Metal Nanoparticles on a Two-Dimensional Catalyst Mat. Storing and Shuttling Electrons with Reduced Graphene Oxide. *Nano Lett.* 2010, *10* (2), 577–583. https://doi.org/10.1021/nl9035109.

(5) Fan, Z.; Yan, J.; Zhi, L.; Zhang, Q.; Wei, T.; Feng, J.; Zhang, M.; Qian, W.; Wei, F. A

Three-Dimensional Carbon Nanotube/Graphene Sandwich and Its Application as Electrode in Supercapacitors. *Adv. Mater.* 2010, *22* (33), 3723–3728. https://doi.org/10.1002/adma.201001029.

(6) Yin, Z.; Zhu, J.; He, Q.; Cao, X.; Tan, C.; Chen, H.; Yan, Q.; Zhang, H. Graphene-Based Materials for Solar Cell Applications. *Advanced Energy Materials*. 2014. https://doi.org/10.1002/aenm.201300574.

(7) Gong, Y.; Lin, J.; Wang, X.; Shi, G.; Lei, S.; Lin, Z.; Zou, X.; Ye, G.; Vajtai, R.; Yakobson, B. I.; Terrones, H.; Terrones, M.; Tay, B. K.; Lou, J.; Pantelides, S. T.; Liu, Z.; Zhou, W.; Ajayan, P. M. Vertical and In-Plane Heterostructures from WS_2 /MoS_2 Monolayers. *Nat. Mater.* 2014, *13* (12), 1135–1142. https://doi.org/10.1038/nmat4091.

(8) Manzeli, S.; Ovchinnikov, D.; Pasquier, D.; Yazyev, O. V.; Kis, A. 2D Transition Metal Dichalcogenides. *Nature Reviews Materials*. 2017. https://doi.org/10.1038/natrevmats.2017.33.

(9) Geim, A. K. Nobel Lecture: Random Walk to Graphene. *Rev. Mod. Phys.* 2011, *83* (3), 851–862. https://doi.org/10.1103/RevModPhys.83.851.

(10) Grønborg, S. S.; Ulstrup, S.; Bianchi, M.; Dendzik, M.; Sanders, C. E.; Lauritsen, J. V.; Hofmann, P.; Miwa, J. A. Synthesis of Epitaxial Single-Layer MoS_2 on Au(111). *Langmuir* 2015, *31* (35), 9700–9706. https://doi.org/10.1021/acs.langmuir.5b02533.

(11) Dendzik, M.; Michiardi, M.; Sanders, C.; Bianchi, M.; Miwa, J. A.; Grønborg, S. S.; Lauritsen, J. V.; Bruix, A.; Hammer, B.; Hofmann, P. Growth and Electronic Structure of Epitaxial Single-Layer WS_2 on Au(111). *Phys. Rev. B - Condens. Matter Mater. Phys.* 2015, *92* (24). https://doi.org/10.1103/PhysRevB.92.245442.

(12) Biener, M. M.; Biener, J.; Friend, C. M. Novel Synthesis of Two-Dimensional TiS_2 Nanocrystallites on Au(111). *J. Chem. Phys.* 2005, *122* (3). https://doi.org/10.1063/1.1826054.

(13) Kolekar, S.; Bonilla, M.; Ma, Y.; Diaz, H. C.; Batzill, M. Layer- and Substrate-Dependent Charge Density Wave Criticality in 1T-$TiSe_2$. *2D Mater.* 2018, *5* (1). https://doi.org/10.1088/2053-1583/aa8e6f.

(14) Tsipas, P.; Tsoutsou, D.; Fragkos, S.; Sant, R.; Alvarez, C.; Okuno, H.; Renaud, G.; Alcotte, R.; Baron, T.; Dimoulas, A. Massless Dirac Fermions in $ZrTe_2$ Semimetal Grown on InAs(111) by van Der Waals Epitaxy. *ACS Nano* 2018, *12* (2), 1696–1703. https://doi.org/10.1021/acsnano.7b08350.

(15) Stan, R. M.; Mahatha, S. K.; Bianchi, M.; Sanders, C. E.; Curcio, D.; Hofmann, P.; Miwa, J. A. Epitaxial Single-Layer NbS_2 on Au(111): Synthesis, Structure, and Electronic Properties. *Phys. Rev. Mater.* 2019, *3* (4). https://doi.org/10.1103/PhysRevMaterials.3.044003.

(16) Tsoutsou, D.; Aretouli, K. E.; Tsipas, P.; Marquez-Velasco, J.; Xenogiannopoulou, E.; Kelaidis, N.; Aminalragia Giamini, S.; Dimoulas, A. Epitaxial 2D $MoSe_2$ ($HfSe_2$) Semiconductor/2D $TaSe_2$ Metal van Der Waals Heterostructures. *ACS Appl. Mater. Interfaces* 2016, *8* (3), 1836–1841. https://doi.org/10.1021/acsami.5b09743.

(17) Sørensen, S. G.; Füchtbauer, H. G.; Tuxen, A. K.; Walton, A. S.; Lauritsen, J. V. Structure and Electronic Properties of in Situ Synthesized Single-Layer MoS_2 on a Gold Surface. *ACS Nano* 2014, *8* (7), 6788–6796. https://doi.org/10.1021/nn502812n.

(18) Ataca, C.; Şahin, H.; Ciraci, S. Stable, Single-Layer MX_2 Transition-Metal Oxides and Dichalcogenides in a Honeycomb-like Structure. *J. Phys. Chem. C* 2012, *116* (16), 8983–8999. https://doi.org/10.1021/jp212558p.

(19) Kibsgaard, J.; Morgenstern, K.; Lægsgaard, E.; Lauritsen, J. V.; Besenbacher, F. Restructuring of Cobalt Nanoparticles Induced by Formation and Diffusion of Monodisperse Metal-Sulfur Complexes. *Phys. Rev. Lett.* 2008, *100* (11). https://doi.org/10.1103/PhysRevLett.100.116104.

(20) Herbschleb, C. T.; Van Der Tuijn, P. C.; Roobol, S. B.; Navarro, V.; Bakker, J. W.; Liu, Q.; Stoltz, D.; Cañas-Ventura, M. E.; Verdoes, G.; Van Spronsen, M. A.; Bergman, M.; Crama, L.; Taminiau, I.; Ofitserov, A.; Van Baarle, G. J. C.; Frenken, J. W. M. The ReactorSTM: Atomically Resolved Scanning Tunneling Microscopy under High-Pressure, High-Temperature Catalytic Reaction Conditions. *Rev. Sci. Instrum.* 2014, *85* (8). https://doi.org/10.1063/1.4891811.

(21) Horcas, I.; Fernández, R.; Gómez-Rodríguez, J. M.; Colchero, J.; Gómez-Herrero, J.; Baro, A. M. WSXM: A Software for Scanning Probe Microscopy and a Tool for Nanotechnology. *Rev. Sci. Instrum.* 2007, *78* (1). https://doi.org/10.1063/1.2432410.

(22) Wagner, C. D. Sensitivity Factors for XPS Analysis of Surface Atoms. *J. Electron Spectros. Relat. Phenomena* 1983, *32* (2), 99–102. https://doi.org/10.1016/0368-2048(83)85087-7.

(23) Kresse, G.; Hafner, J. Ab Initio Molecular Dynamics for Liquid Metals. *Phys. Rev. B* 1993, *47* (1), 558–561. https://doi.org/10.1103/PhysRevB.47.558.

(24) Kresse, G.; Hafner, J. Ab Initio Molecular-Dynamics Simulation of the Liquid-Metalamorphous- Semiconductor Transition in Germanium. *Phys. Rev. B* 1994, *49* (20), 14251–14269. https://doi.org/10.1103/PhysRevB.49.14251.

(25) Kresse, G.; Furthmüller, J. Efficiency of Ab-Initio Total Energy Calculations for Metals and Semiconductors Using a Plane-Wave Basis Set. *Comput. Mater. Sci.* 1996, *6* (1), 15–50. https://doi.org/10.1016/0927-0256(96)00008-0.

(26) Kresse, G.; Furthmüller, J. Efficient Iterative Schemes for Ab Initio Total-Energy Calculations Using a Plane-Wave Basis Set. *Phys. Rev. B - Condens. Matter Mater. Phys.* 1996, *54* (16), 11169–11186. https://doi.org/10.1103/PhysRevB.54.11169.

(27) Hjorth Larsen, A.; JØrgen Mortensen, J.; Blomqvist, J.; Castelli, I. E.; Christensen, R.; Dułak, M.; Friis, J.; Groves, M. N.; Hammer, B.; Hargus, C.; Hermes, E. D.; Jennings, P. C.; Bjerre Jensen, P.; Kermode, J.; Kitchin, J. R.; Leonhard Kolsbjerg, E.; Kubal, J.; Kaasbjerg, K.; Lysgaard, S.; Bergmann Maronsson, J.; Maxson, T.; Olsen, T.; Pastewka, L.; Peterson, A.; Rostgaard, C.; SchiØtz, J.; Schütt, O.; Strange, M.; Thygesen, K. S.; Vegge, T.; Vilhelmsen, L.; Walter, M.; Zeng, Z.; Jacobsen, K. W. The Atomic Simulation Environment - A Python Library for Working with Atoms. *Journal of Physics Condensed Matter*. 2017. https://doi.org/10.1088/1361-648X/aa680e.

(28) Feng, Z. Y.; Yang, Y.; Zhang, J. M. The Structural, Electronic and Magnetic Properties of CoS2 under Pressure. *Solid State Commun.* 2018, *273*, 60–65. https://doi.org/10.1016/j.ssc.2018.02.010.

(29) Perdew, J. P.; Burke, K.; Ernzerhof, M. Generalized Gradient Approximation Made Simple. *Phys. Rev. Lett.* 1996, *77* (18), 3865–3868. https://doi.org/10.1103/PhysRevLett.77.3865.

(30) Blöchl, P. E. Projector Augmented-Wave Method. *Phys. Rev. B* 1994, *50* (24), 17953–17979. https://doi.org/10.1103/PhysRevB.50.17953.

(31) Joubert, D. From Ultrasoft Pseudopotentials to the Projector Augmented-Wave Method. *Phys. Rev. B - Condens. Matter Mater. Phys.* 1999, *59* (3), 1758–1775. https://doi.org/10.1103/PhysRevB.59.1758.

(32) Monkhorst, H. J.; Pack, J. D. Special Points for Brillouin-Zone Integrations. *Phys. Rev. B* 1976, *13* (12), 5188–5192. https://doi.org/10.1103/PhysRevB.13.5188.

(33) Alsén, N. Röntgenographische Untersuchung Der Kristallstrukturen von Magnetkies, Breithauptit, Pentlandit, Millerit Und Verwandten Verbindungen. *Gff* 1925, *47* (1), 19–72. https://doi.org/10.1080/11035892509443177.

(34) Nowack, E.; Schwarzenbach, D.; Hahn, T. Charge Densities in CoS_2 and NiS_2 (Pyrite Structure). *Acta Crystallogr. Sect. B* 1991, *47* (5), 650–659. https://doi.org/10.1107/S0108768191004871.

(35) Davey, W. P. Precision Measurements of the Lattice Constants of Twelve Common Metals. *Phys. Rev.* 1925, *25* (6), 753–761. https://doi.org/10.1103/PhysRev.25.753.

(36) Schimka, L.; Gaudoin, R.; Klimeš, J.; Marsman, M.; Kresse, G. Lattice Constants and Cohesive Energies of Alkali, Alkaline-Earth, and Transition Metals: Random Phase Approximation and Density Functional Theory Results. *Phys. Rev. B - Condens. Matter Mater. Phys.* 2013, *87* (21). https://doi.org/10.1103/PhysRevB.87.214102.

(37) Tersoff, J.; Hamann, D. R. Theory of the Scanning Tunneling Microscope. *Phys. Rev. B* 1985, *31* (2), 805–813. https://doi.org/10.1103/PhysRevB.31.805.

(38) Vanpoucke, D. E. P.; Brocks, G. Formation of Pt-Induced Ge Atomic Nanowires on Pt/Ge(001): A Density Functional Theory Study. *Phys. Rev. B - Condens. Matter Mater. Phys.* 2008, *77* (24). https://doi.org/10.1103/PhysRevB.77.241308.

(39) Fitts, W. P.; White, J. M.; Poirier, G. E. Low-Coverage Decanethiolate Structure on Au(111): Substrate Effects. *Langmuir* 2002, *18* (5), 1561–1566. https://doi.org/10.1021/la0107650.

(40) Liu, Y. F.; Yang, Y. C.; Lee, Y. L. Assembly Behavior and Monolayer Characteristics of OH-Terminated Alkanethiol on Au(111): In Situ Scanning Tunneling Microscopy and Electrochemical Studies. *Nanotechnology* 2008, *19* (6). https://doi.org/10.1088/0957-4484/19/6/065609.

(41) Darling, S. B.; Rosenbaum, A. W.; Wang, Y.; Sibener, S. J. Coexistence of the $(23 \times \sqrt{3})$ Au(111) Reconstruction and a Striped Phase Self-Assembled Monolayer. *Langmuir* 2002, *18* (20), 7462–7468. https://doi.org/10.1021/la020334x.

(42) Huang, H.; Tan, Z.; He, Y.; Liu, J.; Sun, J.; Zhao, K.; Zhou, Z.; Tian, G.; Wong, S. L.; Wee, A. T. S. Competition between Hexagonal and Tetragonal Hexabromobenzene Packing on Au(111). *ACS Nano* 2016, *10* (3), 3198–3205. https://doi.org/10.1021/acsnano.5b04970.

(43) Lundqvist, D.; Westgren, A. Röntgenuntersuchung Des Systems CoS. *Zeitschrift für Anorg. und Allg. Chemie* 1938, *239* (1), 85–88. https://doi.org/10.1002/zaac.19382390110.

(44) Knop, O.; Reid, K. I. G.; Sutarno; Nakagawa, Y. Chalkogenides of the Transition Elements. VI. X-Ray, Neutron, and Magnetic Investigation of the Spinels Co_3O_4, $NiCo_2O_4$, Co_3S_4, and $NiCo_2S_4$. *Can. J. Chem.* 1968, *46* (22), 3463–3476. https://doi.org/10.1139/v68-576.

(45) Franke, A.; Pehlke, E. First-Principles Study of 1,4-Butanedithiol Molecules and Radicals Adsorbed on Unreconstructed Au(111) and Au(100). *Phys. Rev. B - Condens. Matter Mater. Phys.* 2010, *81* (7). https://doi.org/10.1103/PhysRevB.81.075409.

(46) Franke, A.; Pehlke, E. Adsorption and Diffusion of SCH_3 Radicals and $Au(SCH_3)_2$ Complexes on the Unreconstructed Au(111) Surface in the Submonolayer Coverage Regime. *Phys. Rev. B - Condens. Matter Mater. Phys.* 2009, *79* (23). https://doi.org/10.1103/PhysRevB.79.235441.

Chapter 3 – Supporting Information

1. Au(111) exposed to H_2S

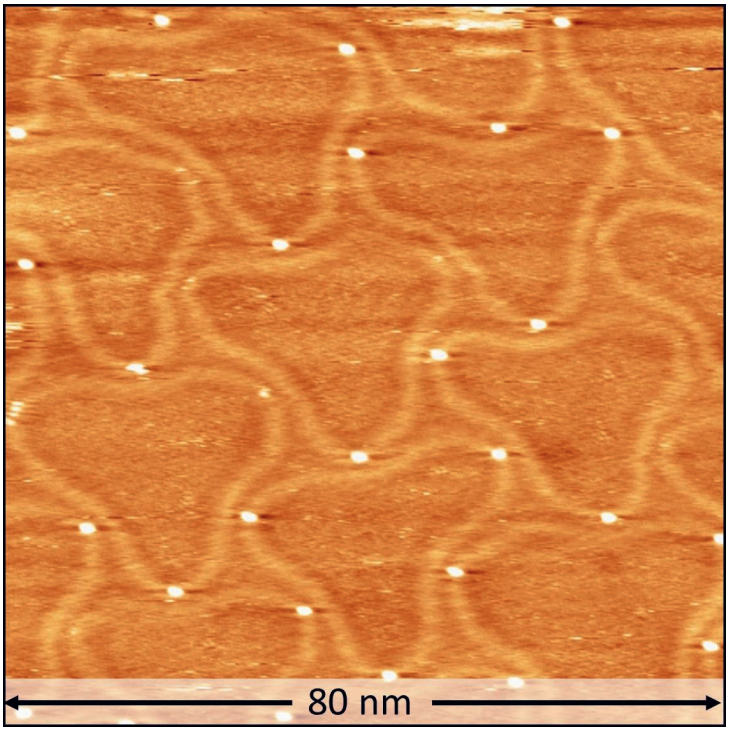

` Figure S1: Modified herringbone reconstruction of Au(111) after exposure to H_2S

The (111) surfaces of metals like Au, Pt and Ir have a tendency to exhibit higher surface atom density than the bulk. In case of Au(111), this shows as the well-known herringbone reconstruction.[S1] When this surface is exposed to H_2S, formation of surface sulfur species causes the herringbone reconstruction to relax and adopt a new structure as shown in S1. This new structure consists of a pair of mirrored 3-point stars arranged as a hexagonal array. A super-saturated Pt gas-phase environment has been observed to induce a similar reconstruction on a clean Pt(111) surface.[S2-S5] This reconstruction of Pt(111) consists of double lines which form star-like features similar to the one observed in our sample. These stars form a network with hexagonal symmetry over large areas of the terrace similar to the reconstruction observed in Figure S1. One key difference is that, in the case of Pt(111), the stars are observed to meet while in the case of Au(111) exposed to H_2S, the double lines do not meet. The Pt(111) surface also shows this behavior in the presence of adatoms such as Co,[S6,S7] Cr[S8] and Cu.[S9]

2. 2D CoS_2 sheets of various sizes supported on Au(111)

At the triple points, the Au(111) step energy is balanced against the step energy of 2D CoS_2 and the Au(111)-2D CoS_2 interfacial energy. This follows from the Young's equation of interfacial tensions,

$$\gamma_{\text{Au step}} = \gamma_{\text{2D } CoS_2 \text{ step}} \cdot \cos\theta + \gamma_{\text{Au-2D } CoS_2 \text{ line interface}} \cdot \cos\varphi \tag{S1}$$

where θ and φ are the respective interfacial angles and γ is the interfacial tension ofthe respective interface at the triple points. We make an assumption that the interfacial tensions are homogeneous in the vicinity of the triple points and hence ignore the torque term (i.e. $d\gamma/d\theta$). For a rigorous quantitative analysis, the torque terms may need to be considered. Figure S2 shows that the corresponding interfacial angles of the two triple points of a 2D CoS_2 sheet display a mirror symmetry. For example, the Au step and the Au-2D CoS_2 line interface has an angle of $158 \pm 0.5^\circ$ at one triple point and $122 \pm 0.5^\circ$ at the other. Such a mirror symmetry could be explained by considering that the 2D CoS_2 step could have different terminations at the two triple points. Further investigations into these phenomena are beyond the scope of this work.

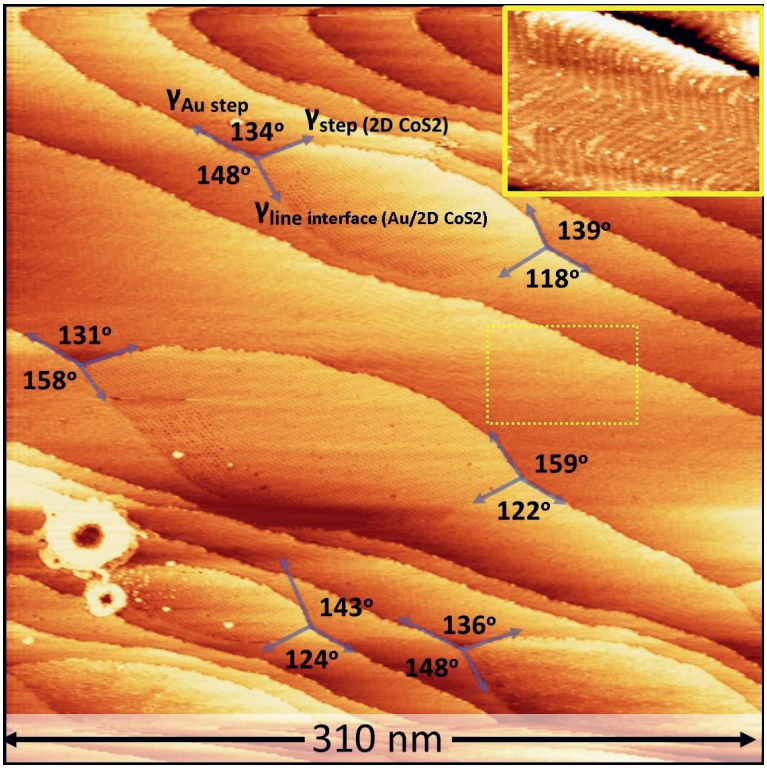

Figure S2: STM images of 2D CoS_2 / Au(111) after flash annealing to 673 K in UHV. The XPS spectra in Figure 2 were measured on this surface. Note the different contact angles at the two triple points of the Au-CoS_2 interface. The herringbone reconstruction, a characteristic of a clean Au(111) surface, is partially restored due to the desorption of most of the sulfur species after the flash annealing (see inset). Bright circular features seen on the lower left corner are debris from the tip as a result of pulsing. Inset shows a zoom-in of the yellow rectangular area.

3. XPS spectra

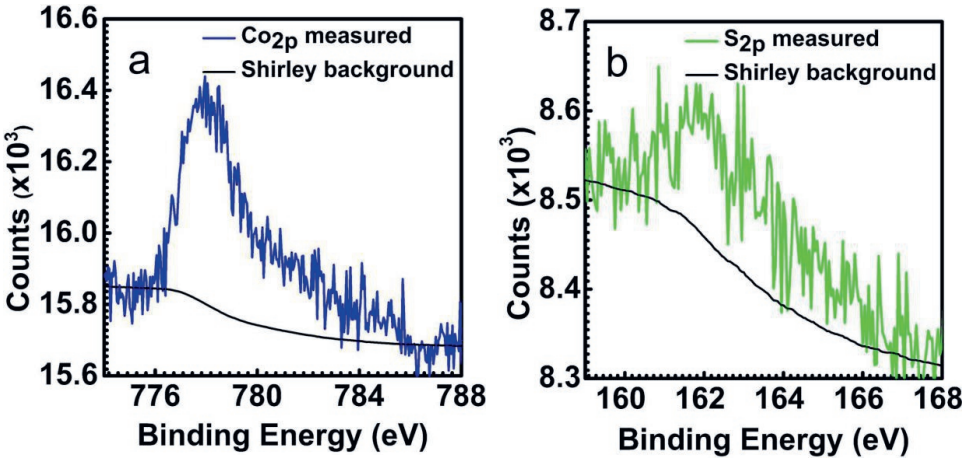

Figure S3: XPS spectra of 2D CoS_2 supported on Au(111) after flash annealing to 673 K to remove sulfur species adsorbed on the Au(111) terraces. (a) Co $2p_{3/2}$. (b) S $2p$.

a. Area under Co $2p_{3/2}$ spectrum = 22923 eV$\times$ counts

R.S.F. of Co $2p_{3/2}$ = 2.8

Contribution of Co taking into account the R.S.F. = $\frac{22983}{2.8}$= 8186.79 eV$\times$ counts;

b. Area under S $2p$ spectrum = 6336 eV$\times$ counts

R.S.F. of S $2p$ = 0.37

Contribution of S taking into account the R.S.F. = $\frac{6336}{0.37}$ = 17124.32 eV$\times$ counts

c. Ratio of Co : S = 8186.79 : 17124.32 $\approx$ 1 : 2.09.

4. TMDC-like structure in sulfur-terminated $Co_3S_4(111)$

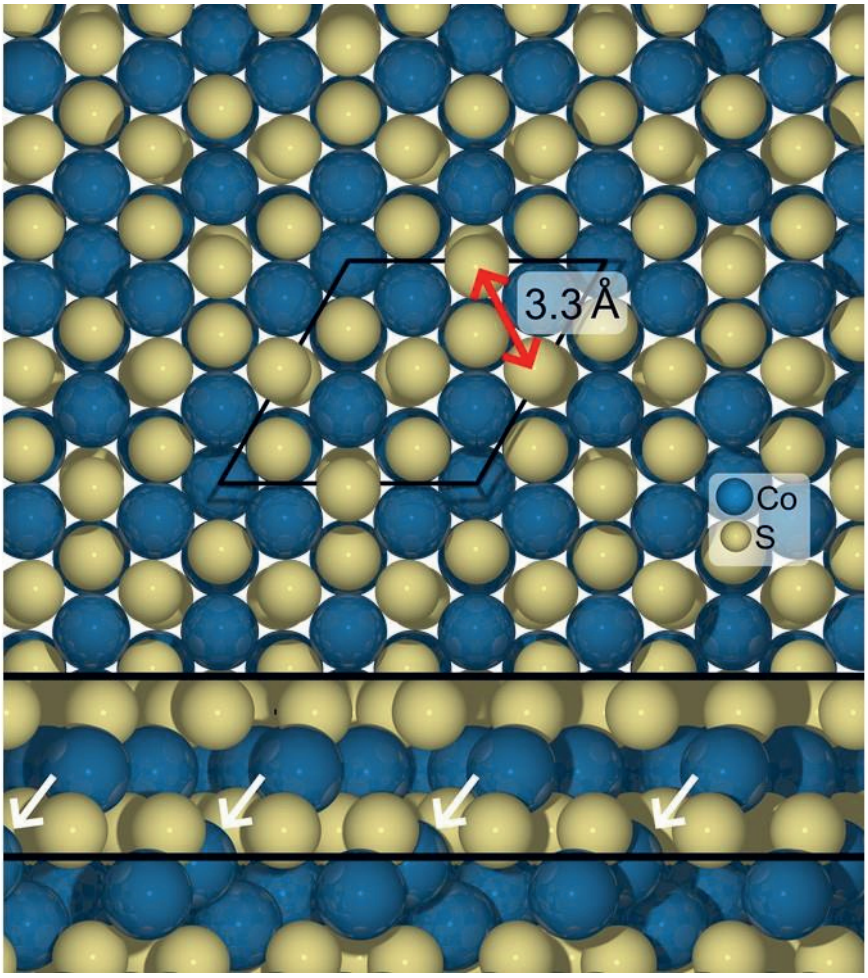

Figure S4: Atomic-scale model for sulfur-terminated $Co_3S_4(111)$ from Lundqvist, D. and Westgren[S11]. Cobalt atoms are shown in blue, while the sulfur atoms are shown in yellow. Top: Top view of the $Co_3S_4(111)$ surface. The hexagonal unit cell of 6.65 A x 6.65 A is indicated in black, however the periodicity of the topmost sulfur layer is half as much(3.33 A, as indicated by the red arrow). Bottom: Side view. The atoms that make up an S-Co-S "sandwich" that form the $Co_3S_4(111)$-cobalt sulfide sheets discussed in this work are enclosed by black lines. The cobalt atoms indicated by white arrows are not part of the proposed structure, resulting in a Co : S = 3 : 8 stoichiometry and visible "holes" in the cobalt layer (see main text).

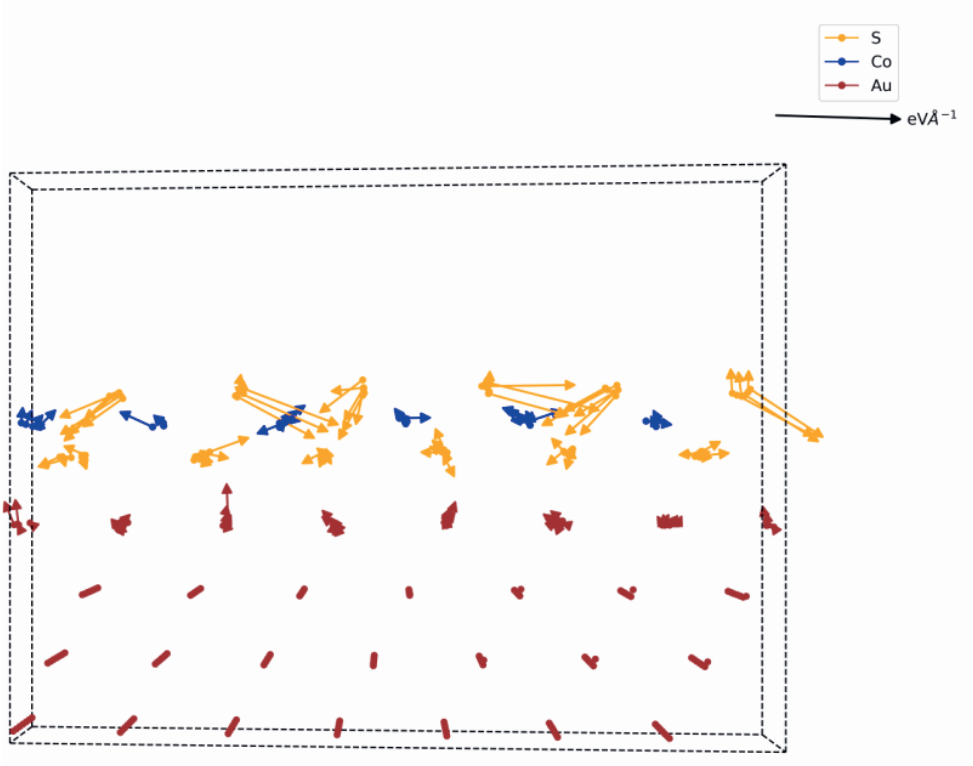

Figure S5: The forces on the atoms in a Co_3S_4(111)-like sheet on Au(111) as suggested by Kibsgaard et al.[S10] at the initial step of the geometry optimization. The length and direction of the arrows are proportional to the magnitude of force. Only forces on the Au atoms in the topmost layer are shown, since the layers below have been frozen in bulk positions. The colors indicate Co (blue), S (orange), and Au (red) respectively.

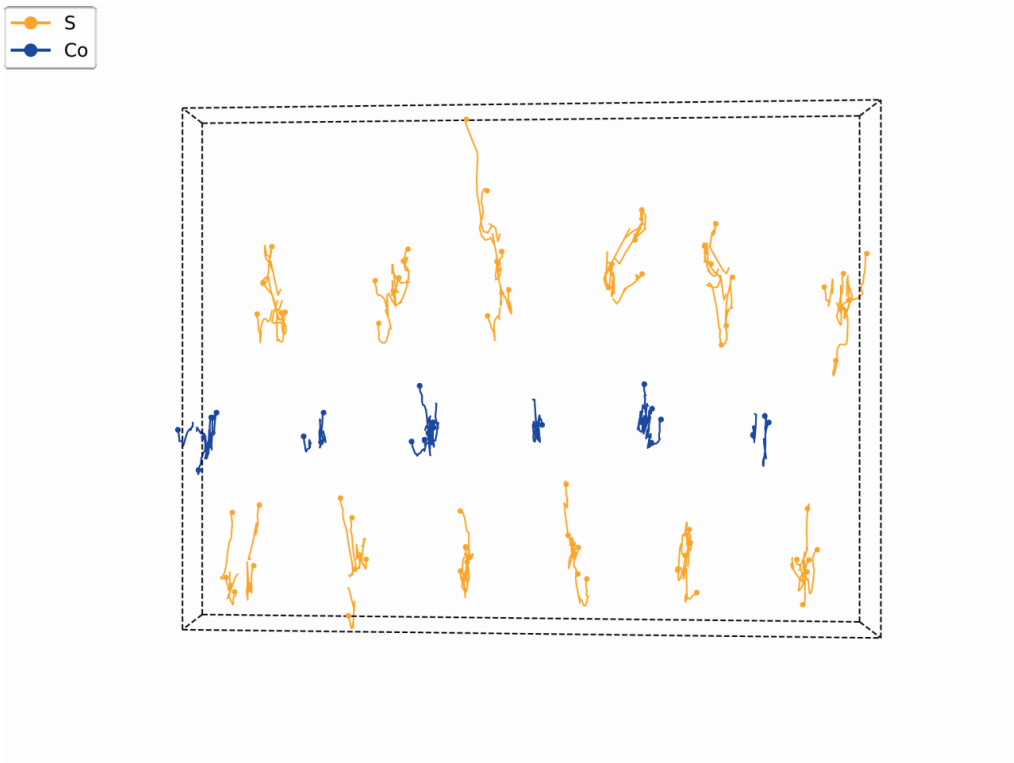

Figure S6: Geometry optimization trajectory for the Co (blue) and S (orange) atoms of a $Co_3S_4(111)$-like sheet on Au(111) as suggested by Kibsgaard et al.[S10] (corresponding to Fig- ure S5). The final position of the atoms is indicated by a circle. The atoms of the Au(111) slab are omitted for the sake of clarity.

The structure suggested by Kibsgaard et al. [S10] consists of a S-Co-S sheet based on $Co_3S_4(111)$, as illustrated schematically in Figure S4. However, our DFT calculations reveal that this structure is not stable. Figure S5 shows that there are large forces on the atoms in the initial step of the geometry optimization. Consequently, the relaxation yields a final structure where the atoms have been significantly displaced from their initial positions as shown in Figure S6.

5. TMDC-like structure in CoS(0001)

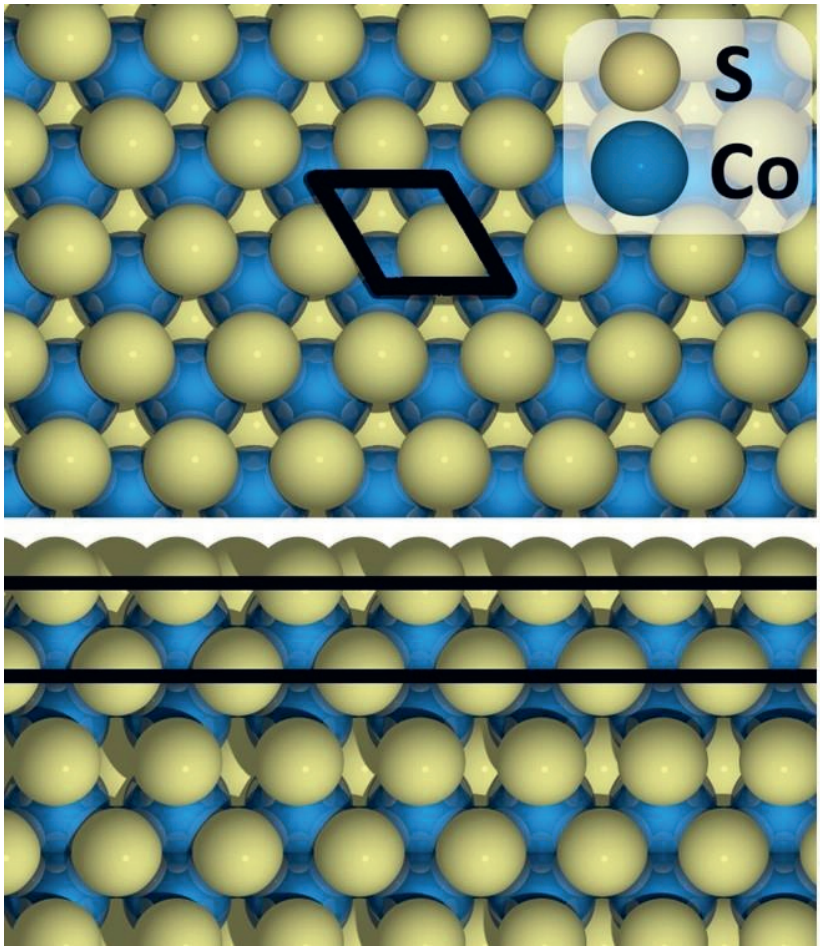

Figure S7: Atomic-scale model for sulfur-terminated CoS(0001). Cobalt atoms are shown in blue, while the sulfur atoms are shown in yellow. Top: Top-down view of the CoS(0001) surface. The hexagonal unit cell of is indicated in black. The experimental lattice constants a_{CoS}^{exp}= 3.38 Å (with a_{Au}^{exp} / c_{Au}^{exp} = 2/3) agree well with those obtained from DFT calculations a_{CoS}^{DFT}= 3.35 Å (with a_{CoS}^{DFT} / c_{CoS}^{DFT} = 2/3). Bottom: Side view.[S12] The atoms that make up the S-Co-S "sandwich" that served as the inspiration for the CoS(0001)-like 2D CoS_2 sheets discussed in this work are enclosed by black lines.

6. Density of states and band structure of 2D CoS_2/Au(111)

In order to compare the electronic band structure of 2D CoS_2 overlayers with large unit cells to freestanding film equivalents and unreconstructed Au(111), we unfold the bands onto the largest surface Brillouin zone according to the method suggested by Popescu and Zunger[S14] as implemented in the BandUp package.[S13,S15] Consistent with STM experiments, in which scanning was possible even at very low bias voltages, the projected densities of states (PDOS) presented in Figure S8 show that the CoS_2 is metallic in contrast to well-studied TMDCs such as e.g. MoS_2. The PDOS also show that both Co and S contribute to the metallic nature of the 2D CoS_2 sheet. In Figure S8, the band structure of the supported CoS(0001)-like 2D CoS_2 sheet on Au(111) from Figure 3c is unfolded and compared to that of the corresponding freestanding 2D CoS_2 sheet as well as a bare Au(111) slab. The 2D CoS_2 states seem strongly affected by the Au at the $\bar{\Gamma}$ point, near the Fermi level, where the bands become more diffuse and hybridize with the nearby gold d-band. The 2D CoS_2 band that is affected the most (indicated by white arrows) exhibits a large p_z-character, indicating hybridization between the p_z-orbital of the sulfur and the d-band of the gold. The hybridization of the 2D CoS_2 states with the d-band of Au is similar to what is reported for MoS_2 sheets on Au(111).[S16]

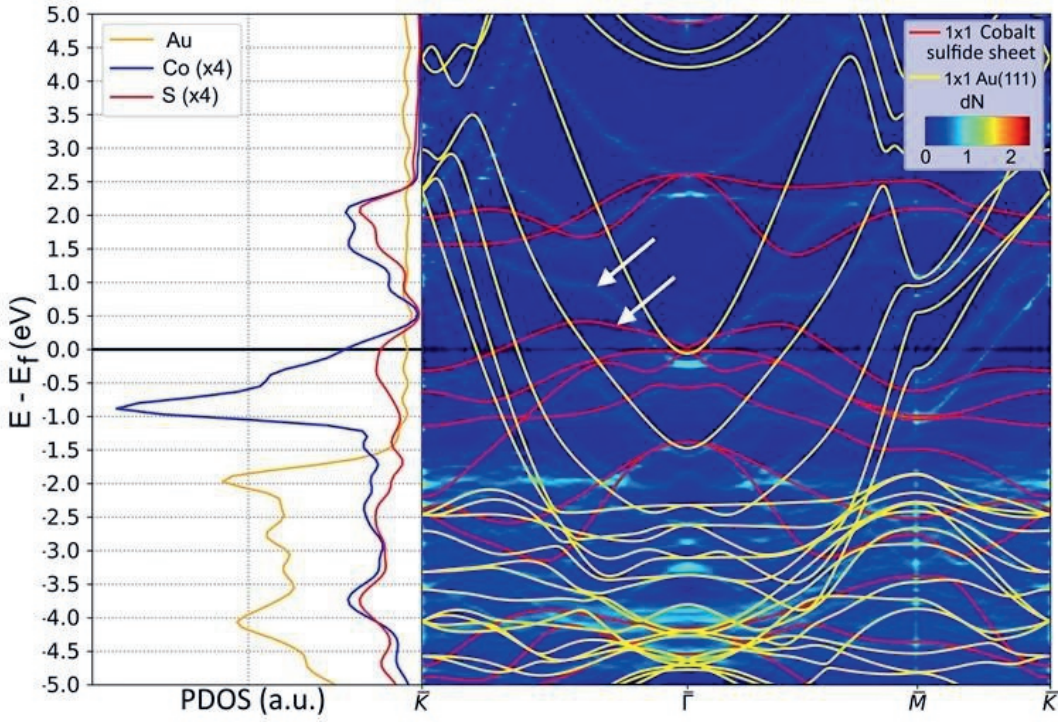

Figure S8: Electronic structure of the CoS(0001)-like 2D CoS_2/Au(111) structure in Figure 3c. Left: Density of states projected on Au (orange), Co (blue), and S (red) atoms. The PDOS of Co and S are multiplied by a factor of 4 for ease of viewing. Right: Comparison of the band structure of gas-phase and Au(111)-supported 2D CoS_2 sheets. The bands of the 2D CoS_2 / Au(111) overlayer structure from Figure 3c are unfolded onto the Brillouin zone of a freestanding CoS(0001)-like 2D CoS_2 film with its much smaller primitive unit cell (background, indicated by color scaleS13). For comparison, the band structure of the latter and the Au(111) slab are shown by the red and yellow lines, respectively. Strong band- hybridization near the $\bar{\Gamma}$ point due to the interaction with the gold surface is indicated by white arrows.

7. Charge analysis

The Bader charges of the corrugated 2D CoS_2 sheet on an Au(111) slab, in vacuum, and of the relaxed sheet in vacuum are compiled in table S1. There is very little difference between the Bader charges of the 2D CoS_2 sheet on the gold substrate and a free-standing 2D CoS_2 sheet (in vacuum), which implies there is little charge transfer between the gold substrate and the 2D CoS_2 sheet. A lack of charge transfer between the sheet and gold indicates their interaction is not ionic in nature. The change in charge density due to the interaction between the CoS_2 sheet and gold substrate is displayed in Figure S9. There is a visible charge depletion near the S- and Au atoms (indicated by red isosurfaces) and there is a charge accumulation in between the S- and Au atoms (indicated by green isosurfaces). This charge accumulation, which is characteristic of covalent-type bonding, is even more obvious in Figure S10, which displays the charge density difference due to the adsorption of the 2D CoS_2 sheet on Au(111) integrated over the surface (xy-) plane.

Table S1: Average Bader charges[S17–S20] for the (relaxed and thus corrugated) 2D CoS_2 on Au(111), the free-standing 2D CoS_2 sheet with the same corrugation as on Au(111), and the free-standing relaxed CoS_2. The average charge accumulation of the sulfur atoms at the bottom of the 2D CoS_2 sheet towards Au(111) and at its top, S_{bottom} and S_{top} respectively, is given separately. Lowest and highest charges are listed in parenthesis.

Element	Average (minimum / maximum) Bader charges (e)				
	CoS_2 sheet on Au(111)		corrugated CoS_2 sheet		CoS_2 sheet
Co	+0.60	(+0.60 / +0.62)	+0.53	(+0.53 / +0.54)	+0.59
S_{bottom}	–0.36	(-0.30 / -0.43)	–0.30	(-0.27 / -0.33)	–0.29
S_{top}	–0.33	(-0.31 / -0.35)	–0.30	(-0.28 / -0.32)	–0.29

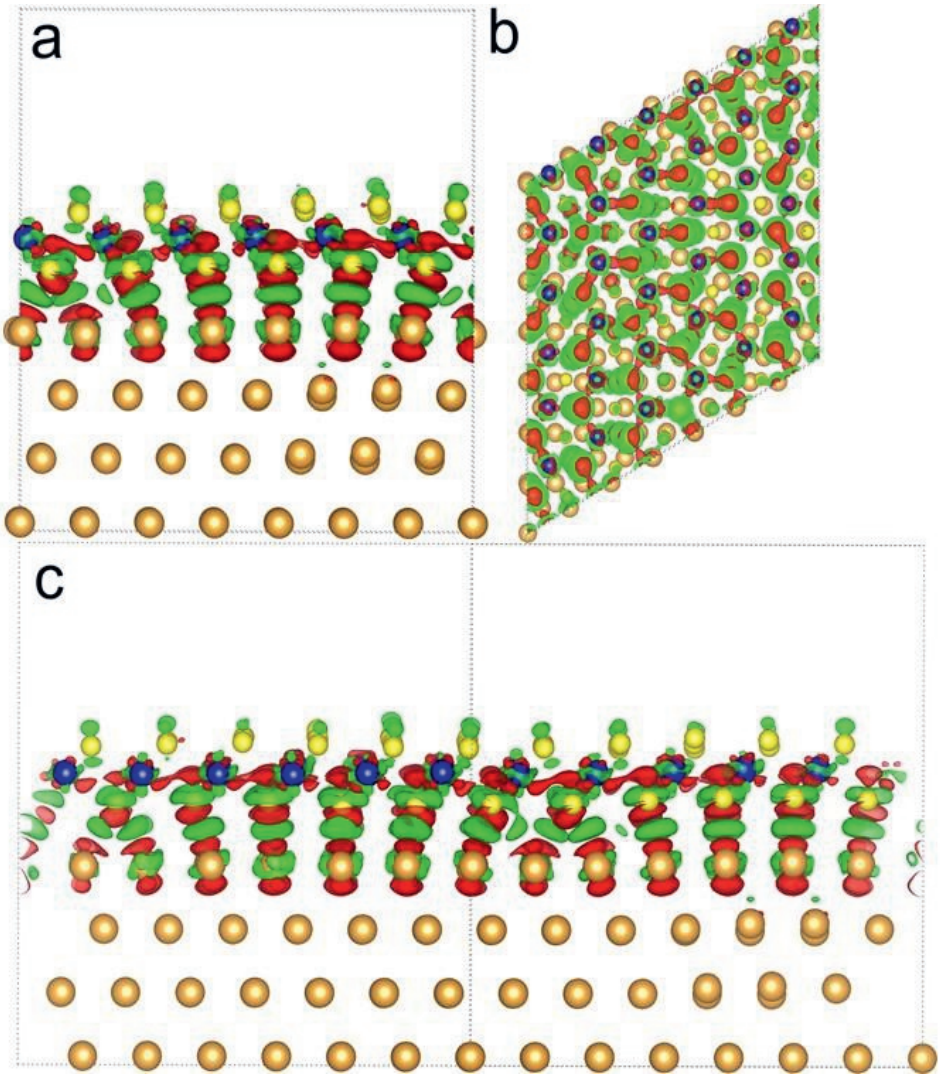

Figure S9: Change in charge density due to interaction between CoS(0001)-like CoS_2 sheet and Au(111) slab. a: Side view. b: Top view c: Side view, rotated by 60°. Gold, cobalt and sulfur atoms are indicated by orange, blue and yellow spheres respectively. A green surface indicates an area of charge accumulation in the combined CoS_2/Au(111), compared to the gas phase, while a red surface indicates an area of charge depletion.

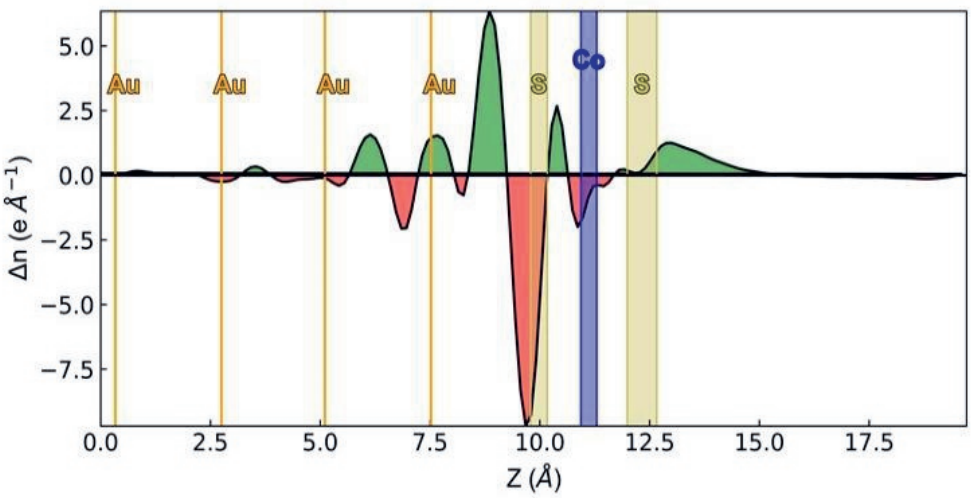

Figure S10: Change in charge density due to interaction between the 2D CoS_2 sheet and Au(111) slab, integrated over the surface (*xy*-) plane. A correction for the dipole intro- duced by the finite periodic cell size in the direction perpendicular to the surface (*z*-direction), resembling that of Neugebauer and Scheffler[S21] is used to avoid unphysical artefacts in the charge density difference. Green indicates charge accumulation, while red indicates charge depletion. The *z*-positions of gold, cobalt and sulfur atoms are marked in orange, blue and yellow respectively. The height variations in the cobalt and sulfur atoms, due to the moire pattern, are indicated in blue and yellow.

8. Van-der-Waals corrections

The influence of van-der-Waals (vdW) forces on the structures was examined by using the D3-method developed by Grimme et al.[S22] on top of our DFT calculations based on the PBE functional, the results of which are presented in the main article.

The adsorption energy of the 2D CoS_2 sheet on Au(111) is -0.98 eV per S-Co-S with PBE+D3, compared to -0.40 eV with PBE (see Figure 5 in the main text). Such a likely overbind- ing has been observed frequently with C_6-correction methods like D3 (see e.g. McNellis et al. [S23]). More importantly, relaxation with PBE+D3 leads to increased corrugation for the structure from Figure 3c. The moire pattern matches the moire pattern obtained using PBE, as demonstrated by the excellent match between Figure S11 and Figure 4 in the main text. Altogether, this is consistent with the bonding to the surface being dominated by covalent interactions between the gold substrate and the sulfur atoms of the 2D CoS_2 structure as analyzed in the previous section 7.

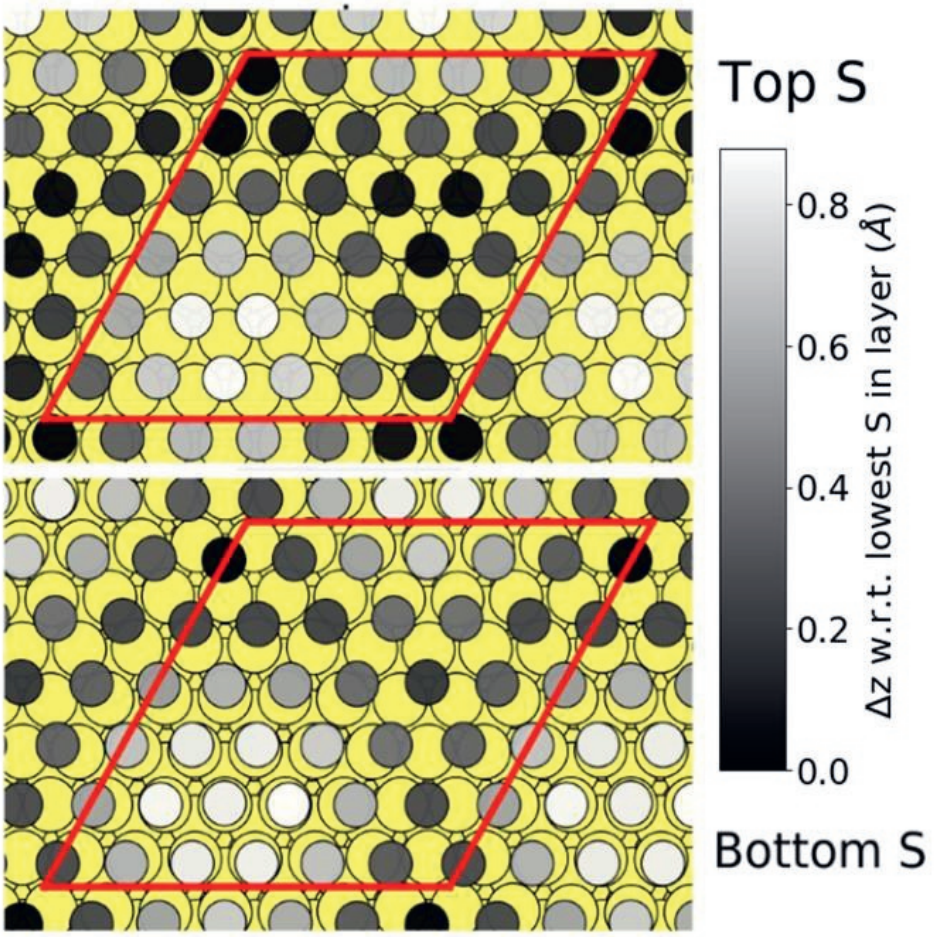

Figure S11: The positions of the sulfur atoms in the top and bottom basal planes of the CoS_2 sheet from Figure 3c. The gold atoms are shown in yellow, while the height of the sulfur atoms relative to the lowest atom in each respective layer is indicated in gray scale. The unit cell is displayed as a red rhombus. The moire pattern looks qualitatively the same as the pattern in Figure 4 in the main text, although the curvature is much stronger.

References

(S1) Chen, W.; Madhavan, V.; Jamneala, T.; Crommie, M. F. Scanning Tunneling Mi- croscopy Observation of an Electronic Superlattice At the Surface of Clean Gold. *Phys. Rev. Lett.* 1998, *80*, 1469–1472.

(S2) Bott, M.; Hohage, M.; Michely, T.; Comsa, G. Pt(111) Reconstruction Induced by Enhanced Pt Gas-phase Chemical Potential. *Phys. Rev. Lett.* 1993, *70*, 1489–1492.

(S3) Hohage, M.; Michely, T.; Comsa, G. Pt(111) Network Reconstruction: Structure, Growth and Decay. *Surf. Sci.* 1995, *337*, 249 – 267.

(S4) Teichert, C.; Hohage, M.; Michely, T.; Comsa, G. Nuclei of the Pt(111) Network Reconstruction Created by Single Ion Impacts. *Phys. Rev. Lett.* 1994, *72*, 1682–1685.

(S5) Sandy, A. R.; Mochrie, S. G. J.; Zehner, D. M.; Gr¨bel, G.; Huang, K. G.; Gibbs, D. Reconstruction of the Pt(111) Surface. *Phys. Rev. Lett.* 1992, *68*, 2192–2195.

(S6) Gr¨tter, P.; D¨rig, U. T. Growth of Vapor-deposited Cobalt Films on Pt(111) Studied by Scanning Tunneling Microscopy. *Phys. Rev. B* 1994, *49*, 2021–2029.

(S7) Gr¨tter, P.; D¨rig, U. Quasidendritic Growth of Co Induced by Localized Reconstruc- tion of Pt(111). *Surf. Sci.* 1995, *337*, 147 – 152.

(S8) Lanping, Z.; Ek, J.; Diebold, U. Highly Ordered Nanoscale Surface Alloy Formed Through Cr-induced Pt(111) Reconstruction. *Phys. Rev. B* 1998, *57*, R4285–R4288.

(S9) Holst, B.; Nohlen, M.; Wandelt, K.; Allison, W. Observation of an Adlayer-driven Substrate Reconstruction in Cu-Pt(111). *Phys. Rev. B* 1998, *58*, R10195–R10198.

(S10) Kibsgaard, J.; Morgenstern, K.; Lægsgaard, E.; Lauritsen, J. V.; Besenbacher, F. Re-structuring of Cobalt Nanoparticles Induced by Formation and Diffusion of Monodis- perse Metal-sulfur Complexes. *Phys. Rev. Lett.* 2008, *100*, 2–5.

(S11) Lundqvist, D. and Westgren, A. Rontgenuntersuchung Des Systems Co-S. *Z. Anorg.*

Allg. Chem. 1936, *48*, 85–88.

(S12) Alsen, N. Rontgenographische Untersuchung Der Kristallstrukturen Von Magnetkies, Breithauptit, Pentlandit, Millerit Und Verwandten Verbindungen. *GFF* 1925, *47*, 19–72.

(S13) Medeiros, P. V. C.; Stafstrom, S.; Bjork, J. Effects of Extrinsic and Intrinsic Perturba- tions on the Electronic Structure of Graphene: Retaining an Effective Primitive Cell Band Structure by Band Unfolding. *Phys. Rev. B* 2014, *89*, 041407.

(S14) Popescu, V.; Zunger, A. Extracting E Versus K Effective Band Structure from Super- cell

Calculations on Alloys and Impurities. *Phys. Rev. B* 2012, *85*, 085201.

(S15) Medeiros, P. V. C.; Tsirkin, S. S.; Stafstrom, S.; Bjork, J. Unfolding Spinor Wave Functions and Expectation Values of General Operators: Introducing the Unfolding- density Operator. *Phys. Rev. B* 2015, *91*, 041116.

(S16) Bruix, A.; Miwa, J. A.; Hauptmann, N.; Wegner, D.; Ulstrup, S.; Grønborg, S. S.; Sanders, C. E.; Dendzik, M.; Grubisic ˇabo, A.; Bianchi, M.; Lauritsen, J. V.; Khaje- toorians, A. A.; Hammer, B.; Hofmann, P. Single-layer MoS_2 on Au(111): Band Gap Renormalization and Substrate Interaction. *Phys. Rev. B* 2016, *93*, 1–10.

(S17) Henkelman, G.; Arnaldsson, A.; J´nsson, H. "A Fast and Robust Algorithm for Bader Decomposition of Charge density". *Comput. Mater. Sci.* 2006, *36*, 354 – 360.

(S18) Sanville, E.; Kenny, S. D.; Smith, R.; Henkelman, G. Improved Grid-based Algorithm for Bader Charge Allocation. *J. Comput. Chem.* 2007, *28*, 899–908.

(S19) Tang, W.; Sanville, E.; Henkelman, G. A Grid-based Bader Analysis Algorithm with- out Lattice Bias. *J. Phys.: Condens. Matter* 2009, *21*, 084204.

(S20) Yu, M.; Trinkle, D. R. Accurate and Efficient Algorithm for Bader Charge Integration. *J. Chem. Phys.* 2011, *134*, 064111.

(S21) Neugebauer, J.; Scheffler, M. Adsorbate-substrate and Adsorbate-adsorbate Interac- tions of Na and K Adlayers on Al(111). *Phys. Rev. B* 1992, *46*, 16067–16080.

(S22) Grimme, S.; Antony, J.; Ehrlich, S.; Krieg, H. A Consistent and Accurate Ab Ini- tio Parametrization of Density Functional Dispersion Correction (DFT-D) for the 94 Elements H-pu. *J. Chem. Phys.* 2010, *132*, 154104.

(S23) McNellis, E. R.; Meyer, J.; Reuter, K. Azobenzene At Coinage Metal Surfaces: Role of Dispersive Van Der Waals Interactions. *Phys. Rev. B* 2009, *80*, 205414.